American Journal of Quantum Chemistry and Molecular Spectroscopy
2019; 3(1): 17-30
http://www.sciencepublishinggroup.com/j/ajqcms
doi: 10.11648/j.ajqcms.20190301.14

Cross Linking-cyanoethylation for Chitosan Polymer for the Removal of Cr(III) and Co(II) Using Batch and Fixed Bed Column Methods

Nada Mohamed Bayomi

Physics and Mathematical Engineering Department, Faculty of Engineering, Egyptian Chinese University, Cairo, Egypt

Email address:
engn412@gmail.com

To cite this article:
Nada Mohamed Bayomi. Cross Linking-cyanoethylation for Chitosan Polymer for the Removal of Cr(III) and Co(II) Using Batch and Fixed Bed Column Methods. *American Journal of Quantum Chemistry and Molecular Spectroscopy.* Vol. 3, No. 1, 2019, pp. 17-30.
doi: 10.11648/j.ajqcms.20190301.14

Received: July 21, 2019; **Accepted**: August 13, 2019; **Published**: September 3, 2019

Abstract: Modified chitosan was prepared by reaction of cross-linked chitosan beads (CLCB) with acrylonitrile via cyanoethylation reaction of amino group which supports chitosan with nitrile groups, then the resulting cyanoethylated chitosan beads (CECB) were converted to chitosan-amidoxime chelating resin (CACR) via reaction with hydroxylamine hydrochloride. The resulted chelating resin was in the form of beads in order to be easy to capture heavy metals from water. Characterization was made using FTIR Spectroscopy, thermal gravimetric analysis (TGA), differential scanning calorimeter (DSC), BET surface area, and scanning electron microscope (SEM). The adsorption of cobalt and chromium from aqueous solution onto CACR has been investigated as a function of pH, metal ion concentration, contact time, metal ion concentration and temperature. Adsorption experiments indicated that the adsorption capacity was dependent on operating variables which are minimally (47.84, 50.68mg/g) and maximally (600, 147.33 mg/g) for Cr(III) and Co(II) respectively. Results revealed that CACR has high affinity toward Co(II) and Cr(III) ions. The saturated adsorption capacities at 25°C were 147.33 and 600 mg/g resin for Co(II) and Cr(III), respectively. Equilibrium isotherm data were analyzed using Langmuir, Freundlich, and Temkin isotherm models for Co(II) and Cr(III). The adsorption was well fitted by Langmuir isotherm model for Co(II) and Cr(III). The kinetic data indicated that adsorption fitted well with the pseudo-second-order kinetic model for Co(II) and Cr(III). Equilibrium distribution coefficient was obtained at different temperatures Thermodynamic parameters showed that the sorption is endothermic, spontaneous and contributes to increase ΔS of the system. The adsorption performance of CACR toward Co (II) and Cr(III) using fixed bed column method was investigated under different conditions. Mathematical models of Adams–Bohart, Thomas and Yoon–Nelson were applied to the experimental data to analyze the column performance. The results fitted well to the Adams–Bohart, Thomas and Yoon–Nelson models.

Keywords: Chitosan, Crosslinking, Cyanoethylation, Cyanoethylated Chitosan Beads, Chitosan-amidoxime Chelating Resin, Adsorption, Chromium, Cobalt

1. Introduction

Chelating resins are a branch of ion-exchange resins which can be able to make direct chemical composition with cations [1-3]. Chelating resins are almost in the form of polymers (exactly co-polymers) which are supported with active functional groups that are responsible for metal ions capture [4]. The chelation ability is directly affected by the chelating group and the polymeric matrix. One of the significant properties of chelating resins is that it's intensive presence in many countries, also their great sorption ability for metal ions enabled them to spread in many applications like [separation of mixtures containing more than one metal] which may be present in low concentration in solution [5]. Onset of environmental pollution in lakes, rivers and oceans is mainly due to advanced industries, drainage and wars which spread toxicity to plants and aquatic organisms by diffusion of heavy metals that are very dangerous, and can be easily transferred to humans and cause great damage to them [6]. This force coming doom forces researchers to find ways to drain wastes. These various methods include [chemical precipitation, membrane process, reverse osmosis and ion exchange [7-9].

Great recommendations for usage of chelating resins among these techniques as they are classified as cheap polymers, have great sorption ability for metal ions, there hardness and thermo stability allow them to resist high temperature and maintain their sorption abilities and their high sorption capacities [10-12]. Fixed bed column is one of the best ways to remove pollutants like azo dyes from aqueous solutions depending on various parameters such as effect of flow rate, mass of adsorbent and influent dye concentration [13]. Cobalt ions are highly toxic for aquatic ecosystems even at low concentrations due to their non-biodegradability and to their tendency to produce severe illnesses upon accumulation in living organisms. Their removal from used industrial water before drainage is an important environmental concern. Current separation techniques include: biological treatments, membrane processes, chemical and electrochemical techniques and adsorption procedures [14]. Chromium is one of the main components of the industrial effluents such as leather tanning, electroplating, textile, metal processing, wood preservatives, paint, pigments, dyeing and steel fabrication. Chromium can present in many oxidation states, Cr(III) and Cr(VI) are the two most stable ones in aqueous media among which the latter is proved to be more toxic to human being and environment [15]. In our previous work different chelating resins bearing amidoxime, imminodiacetate and dithiocarbamate groups were prepared for removal of some metal ions from aqueous solution with high performance [16-20]. The aim of the present study is to prepare a new modified chitosan beads with pendent amidoxime moieties and use it for the removal of Cr(III) and Co(II) from aqueous solution using batch and column techniques. The effects of various parameter like pH value, metal ion concentration, contact time and temperature on adsorption capacity of chelating resin for metal ions will be studied using batch method and will be investigated using Langmuir, Freundlich and Temkin isotherms. Kinetic and thermodynamic parameters of studied metals removal were also estimated. The adsorption performance of CACR toward Cr(III) and Co(II) using column method will be investigated under different conditions and will be analyzed using Adams–Bohart, Thomas and Yoon–Nelson mathematical models.

2. Experimental

2.1. Materials

Chitosan (deacetylation degree 93%) was purchased from oxford Lab Chem (India), glutaraldehyde (GA), acrylonitrile (AN), acetic acid (AA), liquid paraffin (LP), hydroxylamine hydrochloride were purchased from Alpha Chemika (India) and were used directly. Metal salts $CrCl_3.6H_2O$ and $CoCl_2.6H_2O$ were pure grade products of Nice Chemicals Pvt. Ltd., (India) were used as sources for Cr(III) and Co(II) respectively. All the other reagents used in this work were of analytical grade and used as received without purification. De-ionized distilled water was used throughout the experiments.

2.2. Preparation of Cross-linked Chitosan Beads (CLCB)

Cross-linked chitosan beads were prepared according to the method described by Wang et al. [21]. In brief, 10.0 g of chitosan was dissolved in 200 ml aqueous solution of acetic acid (3%) for 48h and then added to a 1000 ml beaker flask containing 200 ml of liquid paraffin, continuously stirred for 20 min at 40°C. After that, the temperature was increased to 60°C, and glutaraldehyde was added as the cross-linking agent, continuous stirring at 300 rpm for 3h to generate the polymeric beads. The resulted beads were washed several times with petroleum ether, ethanol and de-ionized water in sequence to remove any un-reacted fraction and dried at 50°C under vacuum for 24h.

2.3. Preparation of Cyanoethylated Chitosan Beads (CECB)

Cross-linked chitosan beads (CLCB) (5 g) and acrylonitrile (AN) (50 ml) were mixed in 100 ml methanol then acetic acid (0.2 ml, 99.7%) was added to a flask supported with a magnetic stirrer and reflux. The reaction mixture was stirred at 300 rpm for 48h and 75°C. After cooling, CECB was filtered, washed several times with ethanol and water and dried at 50°C under vacuum for 24h.

2.4. Preparation of Chitosan-amidoxime Chelating Resin (CACR)

A suspension of CECB (5 g) and NH_2OH. HCl (4g) in 70ml methanol–water solution (5:1 v/v) was added to a flask equipped with a magnetic stirrer and reflux condenser. About 15 ml of NaOH aqueous solution (7.5 M) was added to this mixture and the pH was kept at 8. The above mixture was stirred for 48h at 70°C. Finally, the resulted CACR beads was filtered out, washed several times with water and ethanol and dried at 50°C under vacuum for 24h.

2.5. Characterization Survey

2.5.1. FT-IR Analysis

Fourier Transform infrared spectra (FTIR) of the prepared resins were obtained with jasco 6100, made in Japan.

2.5.2. Thermal Gravimetric Analysis

Thermo gravimetric analysis experiments (DSC/TG) for the chelating resin were determined using NETZSCH STA 409 C/CD instrument, Germany. The experiment was carried out in a dynamic atmosphere of helium from room temperature to 700°C at heating rate of 10°C /min and a helium flow rate 1ml/min.

2.5.3. Surface Area

Porous structure parameters were characterized by Brunauer–Emmett–Teller (BET) and BJH methods through N_2 adsorption–desorption methods to examine the porous properties of the chelating resin using nitrogen as the adsorbent at 77.35 K. The measurements were carried out using a model NOVA 3200 automated gas sorption system

(Quantachrome, USA).

2.5.4. Scanning Electron Microscope (SEM)

Scanning electron microscope (SEM) was used to observe the surface morphology of the prepared CACR before and after adsorption of Cr(III) and Co(II). Micrographs were obtained using SEM model Bruker X-Flash 410M detector.

2.6. Adsorption of Metal Ions

2.6.1. Capture Metal Ions Using Batch Method

All experiments were performed with 0.1 g resin in 250 ml bottles with 100 ml of single metal ion solution on a temperature controlled shaker at 250 rpm. All experiments were carried out at 25°C except the temperature experiments. The desired pH of solution was adjusted using few drops of 0.1 M HCl and 0.1M NaOH solutions. The concentration of the metal ions in the solution was determined using Perkin Elmer-AAnalyst 200 atomic absorption. Experiments were carried out in triplicate. The adsorption capacity was calculated according to Eq. (1).

$$q = \frac{C_0 - C_e}{W} \times V \quad (1)$$

Where q is the adsorption capacity (mmol/g). C_o and C_e are the initial and the equilibrium concentrations of metal ions (mmol/L), respectively. V is the volume of metal ions solution (L) and W is the weight of dry resin (g). Determination of the optimum pH for adsorption of metal ions by shaking 0.1 g of resin with 100 ml (12mmol/L) metal ion solution for 3h at adjusted pH.

Experiments of adsorption isotherms were performed by shaking 0.1 g of resin with 100 ml of metal ion solution at optimum pH in a concentration ranging from 1.0 to 18mmol/L. After 3h of shaking, the resin was filtered and the remaining metal ion concentration in solution was estimated.

To investigate the adsorption kinetic of the adsorption process, 0.1 g of resin and 100ml of metal ion solution was continuously shaken at optimum pH and concentration at 25°C. The flasks containing the mixtures were withdrawn at different time intervals to determine the remaining concentration of metal ions.

Measurement of metal ion adsorption by the resin as a function of temperature was studied in the temperature range of 25–55°C. Experiments were performed by shaking 0.1 g of resin with 100 ml of metal ion solutions (1.0 mmol/L) under the optimum pH and contact time. After adsorption, the residual concentration of metal ion was determined as described earlier.

2.6.2. Fixed-bed Column Technique

A continuous adsorption experiment was carried out in laboratory-scale glass column (17 cm height and 1.2 cm diameter) filled with chitosan-amidoxime chelating resin, forming a homogeneous and well-packed bed. The performance of fixed-bed column was described through a break-through curve and expressed as the ratio of effluent metal ion concentration over influent metal ion concentration (C_{eff}/C_o) as a function of time (t). For optimizing the column dynamic, adsorption experiments were carried out at different bed heights (1.7, 3.4, 5.1cm), two constant flow rates (0.5, 1ml min^{-1}), 1$mmol^{-1}$ single metal ion concentration and optimum pH at 25°C. First of all, the column was cleaned by enough de-ionized distilled water in an up flow fashion in order to get rid of air bubbles and to rinse the adsorbent. The remaining concentration of metal ions in the effluent was analyzed as previously described.

The performance of the column adsorption processes is based on the break-through curve which is obtained by plotting C_{eff}/C_o Vs time (t), where C_{eff} and C_o are effluent and influent metal ion concentration, respectively (mmol/L). The mass transfer zone (Δt) [22] is given by Eq. (2).

$$\Delta t = t_e - t_b \quad (2)$$

Where t_b is the break-through time (which is the time needed for the increase of metal ion concentration in the effluent to an appreciable value in a sudden way) and t_e is the bed exhaustion time (which is the time needed for the increase of metal ion concentration in the effluent exceeding 99% of the influent concentration [16]).

The length of the mass transfer zone (Zm) [23, 13] is obtained from the break-through curve and is calculated from Eq. (3).

$$Zm = Z\left(1 - \frac{t_b}{t_e}\right) \quad (3)$$

Where Z is the bed height in mm. The total column adsorption capacity (q_{total}) [23, 13] is calculated from Eq. (4).

$$q_{total} = \frac{QA}{1000} = \frac{Q}{1000} \int_{t=0}^{t=t_{total}} (C_{ad})dt \quad (4)$$

Where A is the area under the break-through curve of the plot between C_{ad} (C_{ad}=C_o- $C_{eff.}$) versus time, Q is the flow rate (ml/min) and $t_{tota\ l}$is the total flow time (min). The equilibrium adsorption capacity ($q_{eq(exp)}$)(mmol g^{-1}) [23, 13] is calculated by Eq. (5).

$$q_{eq(exp)} = \frac{q_{total}}{m} \quad (5)$$

Where m is the total dry weight of CACR (g). The total amount of metal ions fed to the column is calculated from Eq. (6) [23, 13].

$$W_{total} = \frac{C_o Q t_{total}}{1000} \quad (6)$$

Where W_{total} is the whole amount of metal ion placed inside the column. Total percentage removal of metal ions is calculated from Eq. (7) [23].

$$\text{Percentage removal (\%)} = \frac{q_{total}}{W_{total}} \times 100 \quad (7)$$

Elution experiments were carried out by placing 1.0 g of CACR in the column then loaded with Cr(III) and Co(II) at flow rate of 0.5 ml/min. The maximum uptake was obtained in the first run, there after the adsorbent was washed by flowing distilled water crossing the column.

3. Results and Discussion

3.1. Synthesis of CACR

CACR is prepared by modification process of chitosan according to the following the steps presented in Figure 1. The first step represents cross linking reaction of chitosan beads using glutaraldehyde as cross linking agent to give CLCB, the second step illustrates cyanoethylation reaction of remaining amino groups of CLCB via reaction with acrylonitrile to give CECB. The final step is reaction of chitosan beads supported nitrile group with NH_2OH. HCl to convert nitrile groups into amidoxime groups, forming CACR.

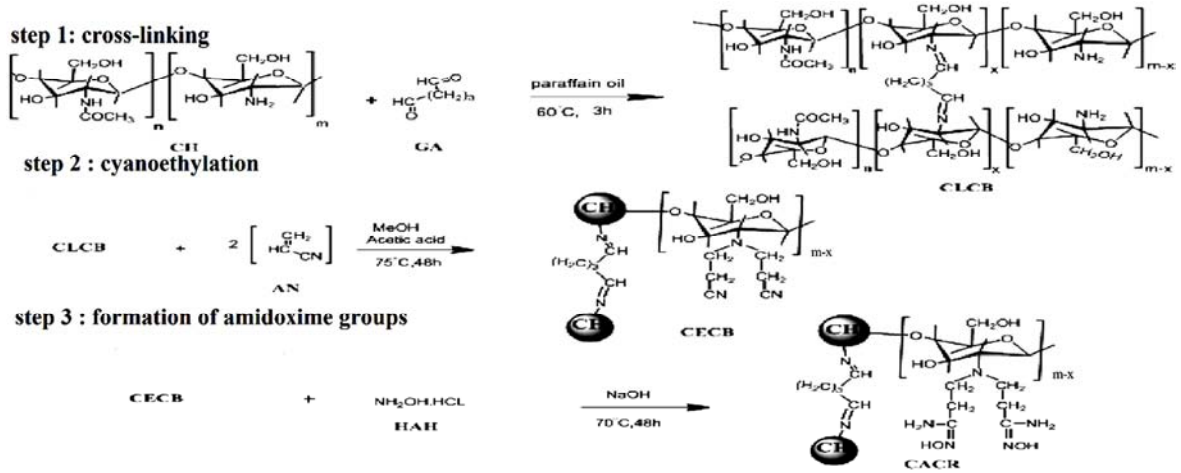

Figure 1. *Preparation steps of chitosan amidoxime chelating resin.*

3.2. Characterization of the Synthesized Resin

3.2.1. FT-IR Analysis

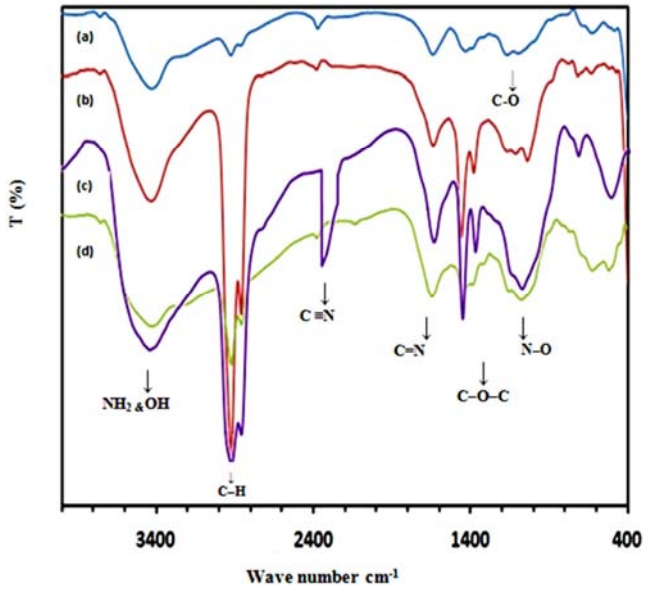

Figure 2. *FTIR spectra of (a) pure chitosan (b) CLCB, (c) CECB and (d) CACR.*

Fourier Transform Infrared absorption spectra of chitosan, CLCB, CECB and CACR is illustrated in Figure 2. Figure 2a shows spectrum of pure chitosan, the –OH and $–NH_2$ (stretching vibration) groups are presented at peak 3427.85cm^{-1} (broad band). The C–O–C bridge absorption band (asymmetric stretching) was observed at 1165.76cm^{-1}, while skeletal vibration of C–O stretching corresponds to the bands at 1095.37 and 1041.37 cm^{-1} [24]. FT-IR spectrum of CLCB (Figure 2b) illustrates stretching vibration bands of C–H (symmetric &asymmetric) which enlarges at 2923.56 & 2858.95cm^{-1} and the peak at 1637.27 cm^{-1} is seen due to imine bonds C=N [25-27]. After reaction with acrylonitrile, a new absorption band appears at 2252.45cm^{-1} which is characteristic of the nitrile vibration band as shown in Figure 2c. Finally FTIR spectrum of CACR (Figure 2d) revealed that the absorption band of the -C≡N group at 2252.45cm^{-1} disappears and a new band at 1075.12 cm^{-1} appears due to the vibration absorption of the N–O bond in the amidoxime group [28].

3.2.2. Thermal Gravimetric Analysis (TGA) of CACR

TGA was applied to illustrate the thermal stability of the chelating resin. The thermo-gram of the CACR is presented in Figure 3 and Table 1. The TGA curve indicates that CACR undergoes degradation in five steps. The first degradation stage ranges from 26 to 220°C with partial weight loss of 19.73% attributable to loss of water molecules which is present in outside surface and internal pores or cavities of the resin. The higher water content ensures the hydrophilic property of the resin. The 2nd stage ranges from 220 to 280°C with partial weight loss 32.64%. As shown in Figure 3 the continuity of heating until 700°C trends to gradual loss of weight which finally reached 6.70%.

Table 1. *TGA and DSC Analysis of CACR.*

TGA	1st degradation step (°C) 26-220	2nd degradation step (°C) 220-280	3rd degradation step (°C) 280-370	4th degradation step (°C) 370-540	5th degradation step (°C) 540-700
DSC	1st Endothermic peak (°C) 204.5	2nd Endothermic peak (°C) 211.5	3rd Endothermic peak (°C) 225.8	4th Endothermic peak (°C) 457.5	5th Endothermic peak (°C) 509.2

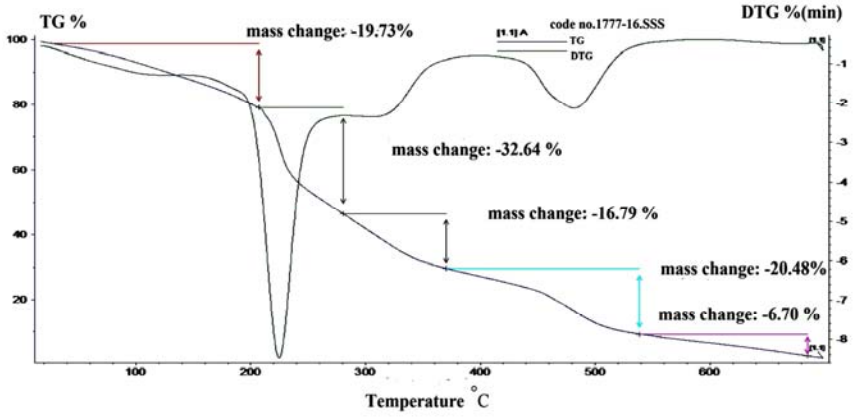

a

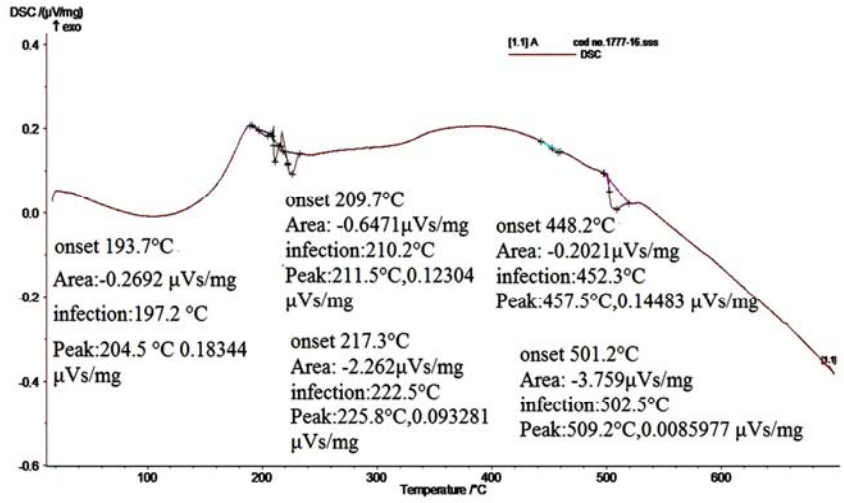

b

Figure 3. *TGA and DSC for CACR.*

Differential scanning calorimeter (DSC) is an excellent tool to measure the thermal stability of the CACR at different temperatures. This device allows quick and accurate results for the thermal stability. The DSC is a direct examination for various heat up-takes between an inert (He) gas as reference and a sample. Five stages heating process were conducted for the DSC analysis in Figure 3a. As shown in Table 1 the first stage heating is used to decrease the water content inside the resin and showed endothermic peak at 204.5°C which indicates the high stability of CACR and its ability to acquire more heat energy [16].

Four other endothermic peaks were shown in Figure 3b due to the continuous heating which represents a large scale, ensures the high stability of CACR as thermal decomposition of resin starts after 509.2°C and there was a trend to total thermal decomposition presented in flat line [16].

3.2.3. Scanning Electron Microscope (SEM)

The surface morphology of CACR is examined by scanning electron microscopy. The scanning electron micrograph images of CACR, CACR-Cr(III) and CACR-Co(II) are shown in Figure 4a, b and c, respectively. The morphology of CACR before metal ion uptake shows clear empty cavities which can help for mass transfer of metal ions to its surface. After metal ion uptake, the resin surface became totally saturated and the cavities disappeared specially in CACR-Cr(III), this means that chromium ions have high adsorption rate than that of cobalt ions, which still contains unfilled cavities [16, 29].

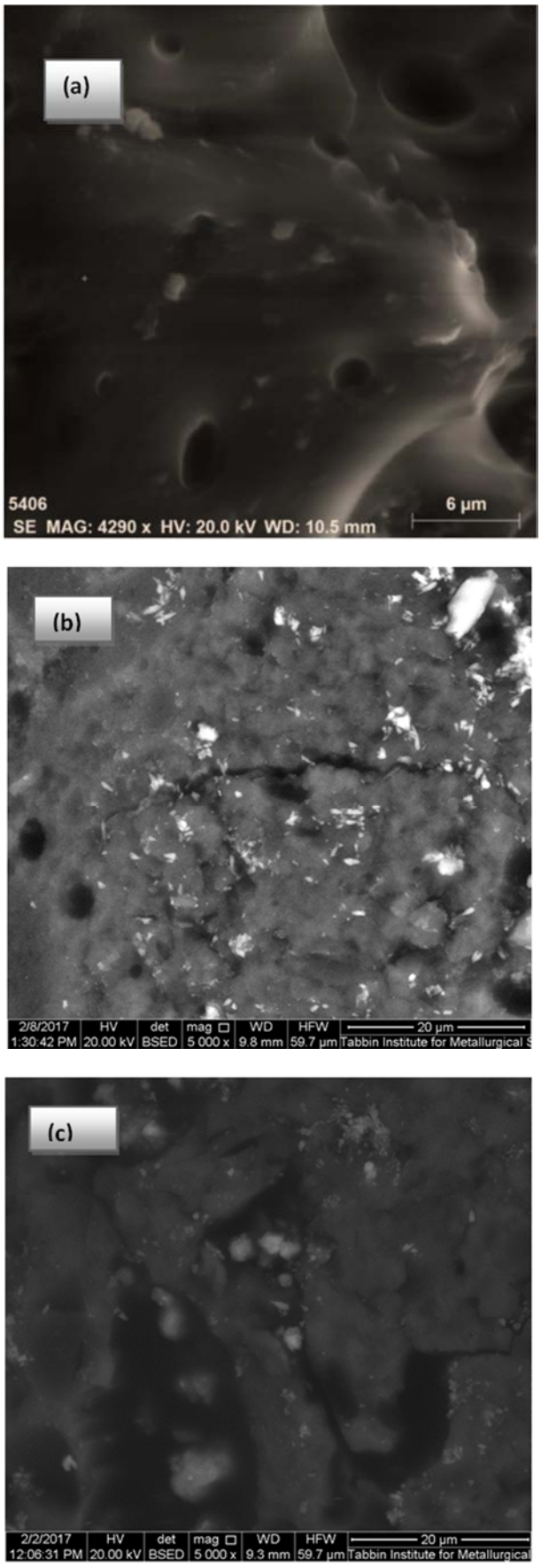

Figure 4. *SEM micrographs of (a)CACR, (b)CACR-Cr and (c) CACR-Co.*

3.2.4. Surface Area

Before examination, the resin was put in vacuum at 300°C for 2 h. by means of adsorption of ultra pure nitrogen at 77.35 K. The surface area was measured using the Brunauer–Emmett–Teller (BET) and BJH method based on adsorption data in the partial pressure (P/P0) range of 0.09–0.29. The total pore volume was determined from the amount of nitrogen adsorbed at P/P0 = 0.29729. Pore size and pore volume were collected in Table 2. These results show that the resin has surface area of 39.52 m^2/g with pore diameter of 2.981nm which to be considered mesoporous structure and lead to efficient transfer the metal ions to the internal adsorption sites [16].

Table 2. *Porous structure parameters of CACR.*

Parameters	Amidoxime
BET surface area (m^2/g)	39.52
BJH desorption average pore diameter (nm)	2.981
BJH desorption cumulative volume of pores (cm^3/g)	0.1405

3.3. Sorption of Metal Ions by Batch Technique

3.3.1. Optimum pH of Metal Ions Uptake

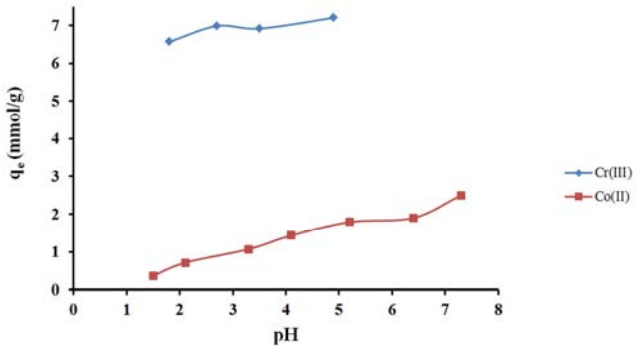

Figure 5. *Effect of pH on the uptake of metal ions at 25°C;shaking time, 3h and initial metal ion concentration of 8 mmol/L.*

The influence of the pH on the uptake capacity of metal ion was examined by batch system at 25°C in the pH range of 1.0–5.0 for Cr(III) and 1.0–7.3 for Co(II) and the results were presented in Figure 5. The amidoxime group (–$C(NH_2)$=N–OH), has amphoteric property [30]. At lower pH value, the basic amino group (–NH_2) lose the ability to make complex with metal ions M(II) since (–NH_2) group blocked and give (–$^+NH_3$), that cause the decrease in metal ion uptake. By increasing pH value, the concentration of H^+ ions decreased therefore protonation of (–NH_2) group will be weakened which cause high chelation of amino group toward metal ions. Also, the level of dissociation of (–OH) group will increase and give ($^-$O) resulting in electrostatic interaction between amidoxime groups of CACR and metal ions, leading to high metal ion sorption [20]. As presented in Figure 5, the adsorption capacity increases when the pH value was increased until it reaches the maximum (optimum value). The optimum pH value which resulted in the greatest adsorption capacity for metal is located at 4.9 and 7.3 for

Cr(III) and Co(II), respectively. Consequently, for this work all the consequent experiments were performed at these optimum pH values. Above these optimum pH, metal is converted to precipitated metal (II) hydroxide and the adsorption of these ions cannot be measured accurately. The possible chelation model of CACR with metal ions is shown in Figure 6.

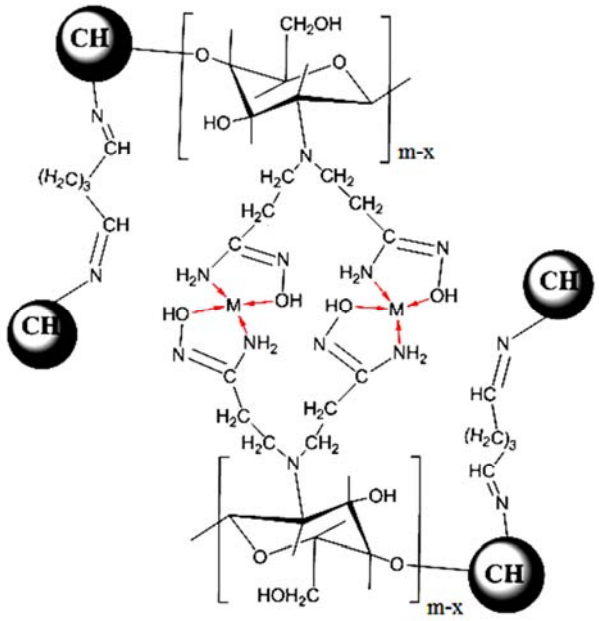

Figure 6. *Chelation of chitosan amidoxime chelating resin for metal ions.*

3.3.2. Effect of Initial Concentration and Equilibrium Isotherm Models

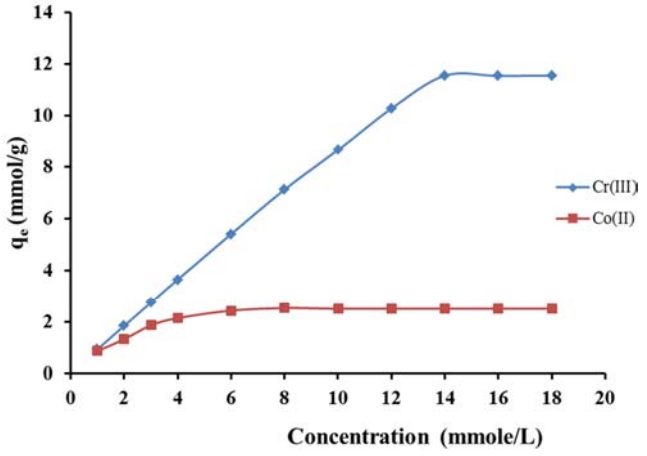

Figure 7. *Effect of initial metal ions concentration on the adsorption capacity of Cr(III) and Co(II); 25°C shaking time 3h and at the optimum pH value.*

The influence of the initial metal ion concentrations on equilibrium adsorption was studied and the results are illustrated in Figure 7. It was obvious from The results that the amount of Cr(III) and Co(II) adsorbed onto CACR increased by the increase of the initial concentration of metal ions before reaching a plateau shape. The maximum adsorption capacity was obtained at optimum pH of each metal ion and at 25°C. The results showed that the maximum adsorption capacity of Cr(III) and Co(II) reached 600 and 147.33 (mg/g), respectively at maximum initial concentration of 14 and 8 (mmol/L). The data presented in literature survey reveals that, generally, the prepared CACR in this work has a good advantage in metal ion adsorption compared to the previously reported adsorbents.

Various adsorption isotherms are valid, the mostly useful models related to the equilibrium characteristics of adsorption: Langmuir, Freundlich and Temkin. The Langmuir isotherm model is based on the adsorption of the mono layer of metal ions onto a homogenous surface of the chelating resin. The linear form of Langmuir adsorption model is represented as [31]:

$$\frac{C_e}{q} = \frac{C_e}{Q_{max}} + \frac{1}{K\,Q_{max}} \quad (8)$$

Where C_e is the equilibrium concentration of metal ions (mmol/L), q is the equilibrium adsorption capacity (mmol/g), Q_{max} (mmol/g) and K (L/mmol) are the maximum adsorption capacity and binding constant, respectively. The parameters of Langmuir model are listed in Table 3. Langmuir isotherm model also defined in terms of the dimensionless parameter known as separation factor (R_L) [32] which is represented as follows:

$$R_L = \frac{1}{1+K\,C_o} \quad (9)$$

Where K is the Langmuir constant (binding constant) and C_o is the initial concentration of metal ion (mmol/L). The value of R_L which is calculated recommends the shape of the isotherm to be unfavorable ($R_L > 1$), linear ($R_L = 1$), favorable ($0 < R_L < 1$), or irreversible ($R_L = 0$) [33, 34]. The calculated values of R_L were between zero and one for all metal ions revealed that the metal ion adsorption onto CACR is favorable. The R_L values decreased as the (C_o) of metal ions increased which showed that the adsorption of metal ions is more effective at higher initial concentration.

The Freundlich isotherm model is an empirical equation which refers to a heterogeneous adsorption system. The Freundlich isotherm model is shown by the following equation [35]:

$$\text{Log}q = N \log C_e + \log K_F \quad (10)$$

Where q is the equilibrium adsorption capacity (mmol/g), C_e is the equilibrium concentration of metal ion (mmol/L), K_F and N are the Freundlich constants for the adsorption capacity (mmol/g) and a measurement of efficiency of adsorption, respectively. The values of K_F& N were (5.86, 1.62) and (0.77, 0.31).

Like R_L values that values of term N presents the nature of isotherm to be unfavorable ($N > 1$), favorable ($0 < N < 1$) or irreversible ($N = 0$). The values calculated for N ranges between (0) and (1) for all metal ions which refers to the simplicity of adsorption process of metal ions onto chelating resin.

The Temkin isotherm model is expressed by the following

equation [36]:

$$q = B \ln K_T + B \ln C_e \quad (11)$$

Where B and K_T are Temkin constants which represent the heat of adsorption & equilibrium binding constant, respectively. B and K_T were (3.18, 0.49) and (11.72, 35.39).

The good fit experimental data with Langmuir, Freundlich, and Temkin isotherm models and high correlation coefficient (R^2) (0.997, 0.995) obtained for these plots indicates the validity of these models to CACR for both metals ions. But Freundlich equation shows better results than Temkin and Langmuir models because of higher correlation coefficient for both metal ions.

Table 3. *The parameters of Langmuir, Freundlich and Temkin isotherms for chelating resin at 25°C*

Metal ion	Langmiur isotherm			Freundlich isotherm			Temkin isotherm		
	Q_{max}	K	R^2	N	K_F	R^2	KT	B	R^2
Cr(III)	18.18	0.71	0.997	0.77	5.86	0.991	11.72	3.18	0.953
Co(II)	2.77	1.89	0.995	0.31	1.62	0.964	35.39	0.49	0.96

3.3.3. Effect of Contact Time on Adsorption Process

In order to determine the influence of contact time between CACR and aqueous solution of Cr(III) and Co(II) ions adsorption, variations of adsorption capacity (q_e) Vs time (15-300 min) were plotted in Figure 8. It was found that, the adsorption of Cr(III) and Co(II) ions from aqueous solution using the adsorbent is continuously increased with time increase, showing that most of the adsorption occurred at the initial stages of the adsorption experiments until reaching equilibrium between two phases after 3h. Therefore, this optimum equilibrium time was selected for the next adsorption experiment.

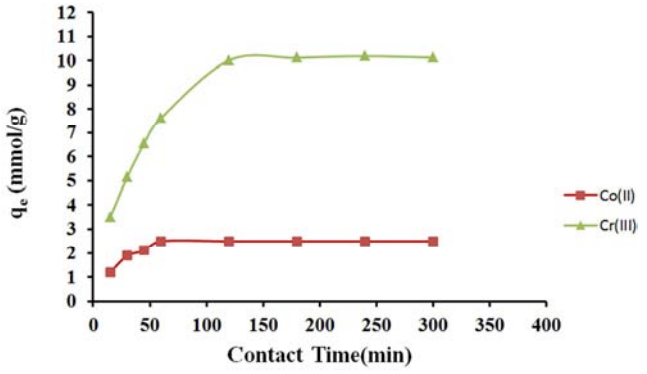

Figure 8. *Effect of contact time on the amount of sorbent of Cr(III) and Co(II) ions on CACR at 25°C, 14,8mmol/L and optimum pH.*

The adsorption results were used to investigate the kinetic mechanism which controls the adsorption process, the most widely used models to described the metal ions using chelating resins are Lagergren's pseudo- first order, pseudo-second order and intra particle diffusion were used to investigate the kinetic process [37-39].

The pseudo-first-order kinetic model is suitable for lower concentrations of metal ions. The linear form of the first order rate equation by Lagergren and Svenska [46] is expressed in Eq. (12):

$$\mathrm{Log}(q - q_t) = \log q - \left(\frac{\mathrm{Kads}}{2.303}\right) t \quad (12)$$

Where q and q_t are the adsorption capacity (mmol/g) at equilibrium and at time t(min), respectively. K_{ads} is the Lagergren rate constant (min^{-1}) of the adsorption.

Plots for Eq. 12 were made for Cr(III) and Co(II) ions sorption at different times. The mathematical linear form of equations used and the plots made for analyzing the data of Lagergren constants regarding to Table 3.

The experimental data were also treated according to pseudo second order kinetic model. The pseudo-second-order model of Ho [40] can be expressed in the linearized form as follows

$$\frac{t}{q_t} = \frac{1}{K_2 q2} + \left(\frac{1}{q}\right) t \quad (13)$$

Where K_2 (g $mmol^{-1}$ min^{-1}) is the pseudo second order rate constant. The constants of the 2nd order kinetic model plots are given in Table 4. Obviously, as it can be seen from the result listed in Table 4, correlation coefficient values (R^2) of the second order kinetic are higher than the values obtained from the first-order kinetics. Therefore, the sorption behavior of Cr(III) and Co(II) onto CACR obeys the second-order kinetics.

Intraparticle diffusion model is described using Eq. 14 proposed by Weber and Morris [41].

$$q_t = K_{id}\, t^{0.5} \quad (14)$$

Where K_{id} is the intraparticle diffusion rate constant (mmol $g^{-1}/min^{0.5}$). The constants of these plots are listed in Table 4. According to Weber and Morris, the adsorbate could be transported from the aqueous phase over adsorbent in three different steps as: (a) Diffusion of metal ions through the boundary layer to the surface of the chelating resin; (b) Intra-particle diffusion: migration of metal ions from the outside surface of the chelating resin to the inside holes or pores of the resin through a pore diffusion or intra-particle diffusion mechanism; and (c) Adsorption of metal ions in an active area on the surface of chelating resin by the effect of chelation.

Table 4. *First-order, second-order and intra particle diffusion rate constants.*

Equations	Parameters	Cr(III)	Co(II)
Pseudo-first order kinetic equation	q(mmol/g)	9.20	2.133
	K_{ads} (1/min)	0.029	0.0391
	R^2	0.988	0.978
Pseudo-second-order kinetics	q(mmol/g)	10.10	2.617
	K_2(gmmol^{-1} min^{-1})	0.0042	0.0378
	R^2	0.997	0.998
Intraparticle diffusion equation	K_{id}(mmol g^{-1} min$^{-1/2}$)	0.389	0.072
	R^2	0.785	0.575

With respect to Eq. 14, if the plot gives a straight line, intra-particle diffusion is accepted as the only rate-limiting step, but multi-linearity is formed which refers to two or more stages related to the adsorption of metal ions [42]. the

adsorption process was restricted by three stages: (1) rapid transportation of metal ions from solution to the resin surface (2) gradual adsorption stage where intra-particle diffusion is rate-limiting step, and (3) final equilibrium stage where intra-particle diffusion begins to slow due to the very low metal ion concentration in the solution, in addition to fewer number of adsorption areas are available. Based on these results, we can conclude that the intra-particle diffusion is not the only step of rate control. This behavior recommends that adsorption processes involve more than one single kinetic stage.

3.3.4. Adsorption Thermodynamics Parameters

Thermodynamic parameters of the adsorption process were examined by performing the adsorption experiments at four various temperatures (25, 35, 45 and 55°C). Metal ion solution (100 ml, 1.0 mmol/L) equilibrated with 0.1 g of CACR at optimum pH value.

Equilibrium distribution coefficient (K_d) for the adsorption process was calculated by Eq. (15) [43].

$$K_d = \frac{C_O - C_e}{C_e} \times \left(\frac{V}{W}\right) \quad (15)$$

Where C_o and C_e are the initial and equilibrium concentration of the metal ions in aqueous solution, respectively (mmol/L), V is the total volume of the solution (L) and W is the weight of the CACR (g).

Free energy change of the adsorption (ΔG°_{ads}) was calculated using the following equation:

$$\Delta G^\circ_{ads} = - RT \ln K_d \quad (16)$$

The standard enthalpy change (ΔH°_{ads}) and entropy change (ΔS°_{ads}) of the adsorption were estimated by plotting $\ln K_d$ versus 1/T according to Eq. (17).

$$\ln K_d = \frac{\Delta S^O_{ads}}{R} + \frac{\Delta H^O_{ads}}{RT} \quad (17)$$

Where R is gas constant (8.314 J/mol K). The values of the slope and the intercept give ΔH°_{ads} and ΔS°_{ads}, respectively. Thermodynamic parameters involving ΔG°_{ads}, ΔH°_{ads} and ΔS°_{ads} for metal ion adsorption onto CACR is illustrated in Table 5. As it can be seen from Table 5, Positive values of ΔH°_{ads} shows that the metal ion adsorption is an endothermic process [44, 45]. Also, the positive values of ΔS°_{ads} may be correlated with the increased randomness due to the liberation of H_2O of hydration during the adsorption of metal ions [44, 45]. Finally, the thermodynamic parameters showed that there is continuity in adsorption process that is indicated by negative values of ΔG°_{ads}.

3.4. Uptake of Metal Ions Using Column Technique

The break-through curves ($C_{eff.}/C_o$ vs. time) were obtained for Cr(III) and Co(II) sorption onto CACR at different bed depth (1.7, 3.4, 5.1 cm), two constant influent flow rates (0.5, 1 ml min^{-1}) and 1mmolL^{-1} single metal ion concentration. The schematic diagram 11 shows the upward movement of the solution through fixed bed column as the cycle starts from automatic burette and by pumping the solution upwardly it reaches the glass column and pass through the resin then collected to be measured. The cycle continues for each bed height and flow rate then changing each one separately. The break-through curves are shown in Figures 9 and 10. The mass transfer zone (Z_m), the sorption capacity of CACR (q_e) and removal percentage (R%) were calculated from the break-through curves by using equations 2-7 and presented in Table 6. According to results, CACR showed a higher adsorption capacity for Cr(III) than Co(II). The maximum sorption capacity was about 1.3962 and 0.24133 mmol g^{-1} for Cr(III) and Co(II) respectively, at flow rate of 0.5ml min^{-1} and bed height of 1.7cm, which corresponds to 89.5% and 73.130% for Cr(III) and Co(II) removal, respectively.

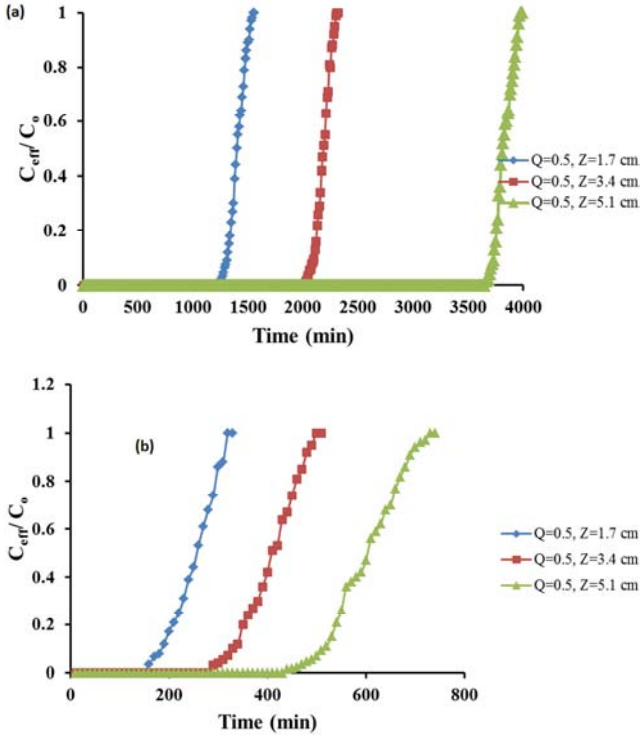

Figure 9. *Break-through curves for (a)Cr(III) and (b) Co(II); initial concentration is 1.0 mmol/l, flow rate is 0.5 ml/min at optimum pH and at 25°C and bed depth (1.7, 3.4, 5.1cm).*

Table 5. *Thermo-dynamic parameters for the adsorption of metal ions onto CACR.*

Metal ion	-ΔG°ads (kJ/mol)				ΔH°ads (kJ/mol)	ΔS°ads (J/mol)	R^2
	298K	308K	318K	328K			
Cr(III)	5.44	7.57	10.28	12.53	66.05	239.53	0.997
Co(II)	1.98	3.094	4.3840	5.7014	35.076	124.12	0.998

Table 6. *Column data parameters, Thomas and Yoon Nelson Models constants at different flow rates and bed heights (C_o = 1 mmol/L).*

Variables			Calculated parameters				Thomas model			Yoon Nelson model			
Metal ion	Q (mL/min)	Z (cm)	q_{total} (mmol)	q_e (mmol/g)	R %	Zm (cm)	q_e (mmol/g)	K_{th} (L/mmol.min)	R^2	K_{YN} (min^{-1})	τ min	R^2	$\tau_{exp.}$ (min)
Cr(III)	0.5	1.7	1.3962	1.3962	89.5	0.318	1.405957	0.01209	0.988254	0.0120896	2052	0.988254	2800
	0.5	3.4	2.17453	1.087265	93.73	0.412	1.0910733	0.0130859	0.975254	0.0130859	4364.29	0.975254	4375
	0.5	5.1	3.81933	1.27311	95.722	0.410	1.277451	0.0114137	0.960365	0.0114137	7664.71	0.960365	7630
	1	1.7	0.47709	0.47709	71.207	1.803	0.483525	0.015491	0.98086	0.015491	483.525	0.98086	495
	1	3.4	0.78801	0.394005	82.948	1.012	0.399722	0.018611	0.985047	0.018611	789.445	0.985047	788
	1	5.1	1.39524	0.46508	90.015	1.092	0.464774	0.019562	0.970373	0.019562	1404.3231	0.970373	1416.667
Co(II)	0.5	1.7	0.24133	0.24133	73.130	0.85	0.25342	0.016626	0.992059	0.016626	506.842	0.992059	513.33
	0.5	3.4	0.39674	0.19837	77.792	1.428	0.20346	0.0147087	0.988992	0.014709	813.836	0.988992	817.78
	0.5	5.1	0.59005	0.1966833	79.736	2.026	0.2001	0.0128182	0.98951	0.012818	1200.77	0.98951	1206.7
	1	1.7	0.14708	0.14708	66.854	0.890	0.158038	0.044267	0.991792	0.044267	158	0.991792	161.25
	1	3.4	0.22433	0.112165	72.364	1.473	0.1176381	0.040696	0.990438	0.040696	235.276	0.990438	237.272
	1	5.1	0.40814	0.136046	81.628	1.561	0.139859	0.036419	0.990103	0.036419	419.576	0.990103	417.273

Table 7. *Adams–Bohart model at different flow rates and bed heights (C_o = 1 mmol/L).*

Variables			Adams–Bohart model		
Metal ion	Flow rate (mL/min)	Z (cm)	kAB (l/mmol .min)	N_0 (mmol/l)	R^2
Cr(III)	0.5	1.7	0.0117	441.15	0.872
	0.5	3.4	0.0135	333.58	0.907
	0.5	5.1	0.0123	383.77	0.8402
	1	1.7	0.0071	367.19	0.9535
	1	3.4	0.0091	267.32	0.8792
	1	5.1	0.0109	294.96	0.9559
Co(II)	0.5	1.7	0.0185	90.20	0.9298
	0.5	3.4	0.0156	69.88	0.9182
	0.5	5.1	0.0139	66.99	0.8874
	1	1.7	0.0216	119.68	0.9321
	1	3.4	0.0194	84.26	0.8896
	1	5.1	0.0184	93.07	0.8939

3.4.1. Effect of Bed Height

The break-through curves of sorption of Cr(III) and Co(II) are shown in Figures 9 and 10. As shown in Figures 9 and 10 the shape of break-through curves of sorption of Cr(III) and Sr (II) at both 0.5 and 1ml min^{-1} flow rates are significantly different as depth changed from 1.7 to 5.1 cm. It was observed that the break-through time and exhaustion time were increased with increased in bed heights [53-54]. This may be due to the amount of resin was more to contact with Cr(III) and Co(II) metal ions. At higher bed heights a larger volume of metal solution could be treated as shown in Table 6 due to increase in the ratio of the resin where more active binding areas are available for processing the sorption process. The break-through time t_b, exhaustion time t_e, the height of mass transfer zone (Z_m) and percentage removal (R%) increased with rise in bed height. The increase in percentage removal must be related to the maximum saturation of all active sites in the adsorbent dosage by metal ions and broad ended mass transfer zone. The decreasing of uptake capacities by increasing the bed height is due to the change in volume to mass ratio [46-47].

3.4.2. Effect of Flow Rate

It was observed that the column performance is excellent at low flow rate. At higher flow rate, the break-through time and exhaustion time reached more rapid and this may be due to the inadequate residence time of the metal ion of Cr(III) and Co(II) with the resin [48]. The result reveals that the break-through curve becomes steeper as the flow rate increased. The metal sorption capacity decreases with the increase of flow rate (Table 6). This is because a much longer time is needed between the solute and that of the solid phase to reach equilibrium state. Therefore, this increase in flow rate causes a shorter presence time of the solute in the column and so, the metal ion leaves the column before equilibrium occurs [49]. Hence break-through time, bed exhaustion time, and sorption capacity were more at 0.5ml min^{-1} when compared to 1ml min^{-1} flow rate.

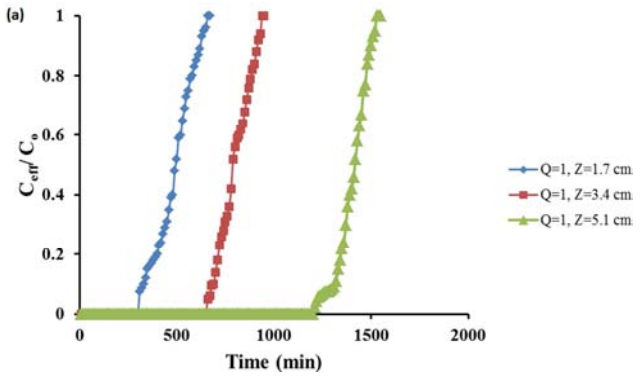

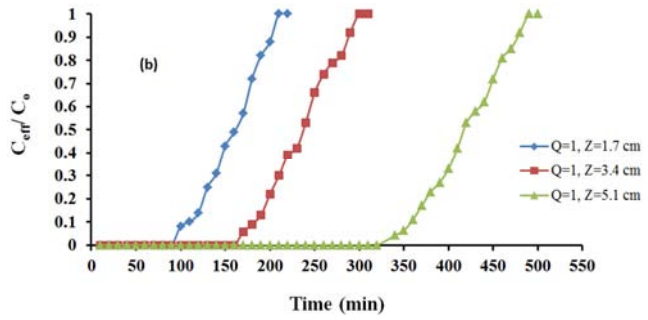

Figure 10. *Break-through curves for (a) Cr(III) and (b) Co(II); initial concentration is 1.0 mmol/l, flow rate is 1 ml/min at optimum pH and at 25°C and bed depth (1.7, 3.4, 5.1cm).*

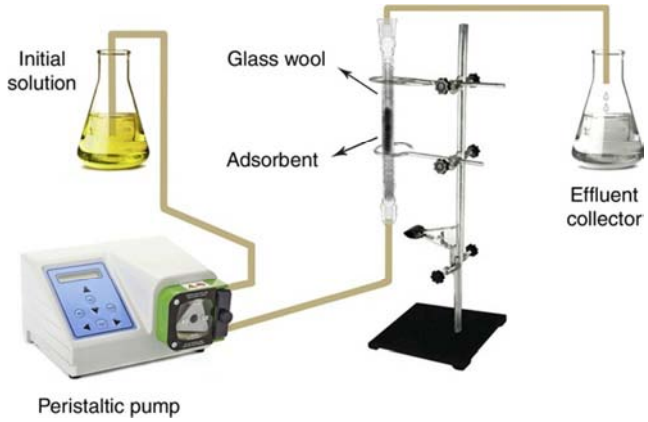

Figure 11. *Fixed bed column technique.*

3.4.3. Modeling of Column Experimental Data

Various theoretical models such as Thomas and Yoon-Nelson models [49-51] were tested to show the experimental data related to the solute interaction behavior and to estimate the break-through curves.

i. The Adams–Bohart model

Adams and Bohart proposed a model based on the surface reaction theory, which assumes the adsorption rate as a function of both the residual capacity of the adsorbent and the concentration of adsorbate species. This model was applied for the description of initial parts of breakthrough curves [52-54]. The Adams–Bohart equation can be expressed by Eq. (18):

$$\ln\frac{C_{eff}}{C_O} = k_{AB}C_0t\_k_{AB}N_0\frac{Z}{U_0} \quad (18)$$

where C_0 and C_t (mmol/l) stand for the inlet and effluent dye concentration, k_{AB} (l/mmol min) is designated as the rate coefficient, U_0 (cm/min) represents the linear velocity defined as the volumetric flow rate to the cross-sectional area of column bed, Z (cm) is the bed height, and N_0 (mmol/l) stands for the sorption capacity of the adsorbent per unit volume of the bed. A linear plot of $\ln(C_t/C_0)$ against t was employed for the adsorption experimental data ranging from 0.5 to 1 in order to determine the model parameters k_{AB} and N_0 (the figure is not shown). These parameters can be calculated from the intercept and the slope of the plot. The values of the k_{AB} and N_0 for all of the breakthrough curves are presented in Table 7, as well as the corresponding correlation coefficient of the model. According to Table 7, the values of k_{AB} increased with increasing flow rate. The values of correlation coefficient are at about 0.9 which represents the suitability of the model for the description of the breakthrough curves at the early parts of the adsorption.

ii. Thomas model

The obtained data from the experiments were used to measure the adsorption capacity of CACR and the adsorption rate constant using Thomas model [55] based on Eq. (19).

$$\ln\left(\frac{C_o}{C_{eff}}-1\right) = \left[\frac{K_{Th}\,q_e m}{Q} - \frac{K_{Th}\,C_O\,V_{eff}}{Q}\right] \quad (19)$$

Where K_{TH} is the Thomas rate constant (l/mmol. min), m is the total dry weight of CACR (g), V_{eff} is effluent volume, q_e is the adsorption capacity of Cr(III) and Co(II) ions on CACR (mmol/g). The linearized form of Thomas model is given by Eq. (20).

$$\ln\left(\frac{C_o}{C_{eff}}-1\right) = \left[\frac{K_{Th}\,q_e m}{Q} - \frac{K_{Th}\,C_O\,V_{eff}}{Q}\right] \quad (20)$$

To detect maximum adsorption capacity of the adsorbent (q_e) and kinetic coefficient (K_{Th}) in Thomas model, experimental data were fit into the Eq. 19. This equation was used to fit the experimentally obtained data by plotting $\ln\left(\frac{C_o}{C_{eff}}-1\right)$ against the effluent volume. The Thomas rate constant and the ion exchange capacity were determined from the slope and intercept, respectively. The values of these two parameters are given in Table 6 for Cr(III) and Co(II) at 10% saturation. According to Table 6 the calculated q_e from Thomas model is similar to the experimental q_e and the value of q_e decreased with increasing both flow rate and bed height. As can be observed, the experimental data are in good agreement with theoretical results.

iii. Yoon Nelson model

The Yoon Nelson model [56] expressed by Eq. (21) is based on the concept of the decrease in the adsorption for each adsorbate molecule is directly proportional to the probability of adsorbate breakthrough on the adsorbent.

$$\frac{C_{eff}}{C_o - C_{eff}} = \exp(K_{YN}t - \tau K_{YN}) \quad (21)$$

K_{YN} is the Yoon Nelson rate velocity constant (L/min), τ is the time in (min) required for 50% adsorbate breakthrough.

The linearized form of Yoon Nelson model is given by Eq. (22).

$$\ln\left(\frac{C_{eff}}{C_o - C_{eff}}\right) = \frac{K_{YN}}{Q}V_{eff} - \tau K_{YN} \quad (22)$$

To determine the rate constant (K_{YN}) and the time needed for 50% adsorbate breakthrough, (τ) in Yoon Nelson model, experimental data were fit into the Eq. 21 This equation was used to fit the experimentally obtained data by plotting $\ln\left(\frac{C_{eff}}{C_o - C_{eff}}\right)$ against the effluent volume. The Yoon Nelson rate constant and time required for 50% adsorbate breakthrough (τ) were determined from the slope and intercept respectively. The values of two

parameters are given in Table 6 for Cr(III) and Co(II) at 50% breakthrough curve. The data in Table 6 also indicate that the τ value of model as similar to the τ_{exp} where τ_{exp} is the time required for 50% adsorbate breakthrough from experiments in min. It was found that the time required for 50% adsorbate breakthrough (τ) for Cr(III) and Co(II) increased with increasing bed height but decreased with increasing flow rate due to less residence time of metal ions in adsorbent bed. Since, the experimental data goes well with the model. Therefore; Yoon Nelson model is suitable model to describe fixed bed operations.

4. Conclusion

A new modified chitosan resin with pendent amidoxime moieties (CACR) was prepared by reaction of cross-linked chitosan beads with acrylonitrile to support the polymer with nitrile group that facilities the reaction of beads with hydroxylamine hydrochloride. Synthesized CACR is characterized using FTIR, thermal gravimetric analysis, SEM, surface area. This resin have high sorption capacity for Co(II) and Cr(III) from their aqueous medium. The sorption of metal ions onto CACR is influenced by several factors such as the solution pH, concentration of metal ions, contact time and solution temperature. In batch equilibrium adsorption method, the optimum sorption pH for Co(II) and Cr(III) were 7.3 and 4.9 respectively. The maximum adsorption capacity of CACR followed the order Cr (III) > Co(II). For Chromium and Cobalt ions, Langmuir isotherm model was the best to indicate the adsorption process also the kinetic experiments showed that adsorption well presented by pseudo-second order model. Thermodynamic parameters also showed that adsorption of metal ions on CACR is spontaneous and endothermic in nature. CACR isn't only efficient for Cr(III) and Co(II) removal by batch but also by column methods, and the best condition for adsorption process at 0.5ml/min and 1.7 cm bed height. Adams-Bohart, Thomas and Yoon Nelson models are suitable models to describe fixed bed column operations.

References

[1] S. C. Apte, G. E. Batley, Trace metal speciation of labile chemical species in natural waters and sediments: non-electrochemical approaches, Anal. Phys. Chem. Environ. Syst. 3 (1995) 259-306.

[2] B. S. Garg, Sharma, R. K. Bhojak, N. Mittal. Chelating Resins and Their Applications in the Analysis of Trace Metal Ions, J. Microchem. 61 (1999) 94-114.

[3] Sharma, R. K. Mittal, S. Koel, Analysis of trace amounts of metal ions using silica-based chelating resins: A green analytical method, Crit. Rev. Anal. Chem. 33 (2003) 183-197.

[4] S. K. Sahni, J. Reedijk, Coordination chemistry of chelating resins and ion exchangers, Coord. Chem. Rev. 59 (1984) 1-139.

[5] C. Liu, Chelating resins in analytical chemistry, Journal of the Chinese Chemical Society. 36 (1989) 389-401.

[6] J. H. Duffus. Heavy metals" – a meaningless term? Pure Applied Chemistry. 74 (2002) 793-807.

[7] M. A. Tofighy, T. Mohammadi, Adsorption of divalent heavy metal ions from water using carbon nanotube sheets, J. Hazard. Mater. 185 (2011) 140–147.

[8] H. Deligz, E. Erdem, Comparative studies on the solvent extraction of transition metal cations by calixarene, phenol and ester derivatives, J. Hazard. Mater. 154 (2008) 29–32.

[9] H. Bessbousse, T. Rhlalou, J. F. Verche`re, L. Lebrun, Removal of heavy metal ions from aqueous solutions by filtration with a novel complexing membrane containning poly(ethyleneimine) in a poly(vinyl alcohol) matrix, J. Membr. Sci. 307 (2008) 249–259.

[10] R. Kumar, M. Kumar, R. Ahmad, M. A. Barakat, L-Methionine modified Dowex-50 ion-exchanger of reduced size for the separation and removal of Cu(II) and Ni(II) from aqueous solution, Chem. Eng. J. 218 (2013) (32–38).

[11] N. Wu, Z. Li. Synthesis and characterization of poly (HEA/MALA) hydrogel and its application in removal of heavy metal ions from water, Chem. Eng. J. 215–216 (2013) 894–902.

[12] Z. Lin, Y. Zhang, Y. Chen, H. Qian. Extraction and recycling utilization of metal ions (Cu^{2+}, Co^{2+} and Ni^{2+}) with magnetic polymer beads, Chem. Eng. J. 200 (2012) 104–110.

[13] M. F. Dahr, M. Esmaieli, H. Abolghasemi, A. Shojamoradi, E. S. Pouya, Continuous adsorption study of congo red using tea waste in a fixed-bed column, Desalination Water Treat. 57 (2016) 8437–8446.

[14] M. A. Barakat, New trends in removing heavy metals from industrial wastewater, Arabian Journal of Chemistry 4 (2011) 361-377.

[15] E. Nieboer, AA Jusys In: Nriagu JO, Nieboer E (eds) Chromium in the natural and human environments, Wiley (1988).

[16] A. F. Shaaban, T. Y. Mohamed, D. A. Fadel, N. M. Bayomi, Removal of Ba(II) and Sr(II) ions using modified chitosan beads with pendent amidoxime moieties by batch and fixed bed column methods, Desalination Water Treat. 82 (2017) 131–145.

[17] A. F. Shaaban, D. A. Fadel, A. A. Mahmoud, M. A. Elkomy, S. M. Elbahy, Synthesis of a new chelating resin bearing amidoxime group for adsorption of Cu(II), Ni(II) and Pb(II) by batch and fixed-bed column methods, J. Environ. Chem. Eng., 2 (2014) 632–641.

[18] A. F. Shaaban, D. A. Fadel, A. A. Mahmoud, M. A. Elkomy, S. M. Elbahy. Removal of Pb(II), Cd(II), Mn(II) and Zn(II) using iminodiacetate chelating resin by batch and fixed bed column methods, Desalination Water Treat., 51 (2013) 5526–5536.

[19] D. A. Fadel, S. M. El-Bahy, Y. A. Abdelaziza, Heavy metals removal using iminodiacetate chelating resin by batch and column techniques, Desalination Water Treat., 57 (2016) 25718–25728.

[20] A. F. Shaaban, D. A. Fadel, A. A. Mahmoud, M. A. Elkomy, S. M. Elbahy, Synthesis and characterization of dithiocarbamate chelating resin and its adsorption performance towards Hg(II), Cd(II) and Pb(II) by batch and fixed-bed column methods, J. Environ. Chem. Eng., 1 (2013) 208–217.

[21] D. F. Wang, B. J. Liu, Y. Xu, L. Zhang. Chinese patent: 201010119859.6.

[22] H. Kalavathy, B. Karthik, LR. Miranda, Removal and recovery of Ni and Zn from aqueous solution using activated carbon from Heveabrasilliensis; batch and column studies, Colloids Surf. B. 78 (2010) 291-302.

[23] Futalan, C. M., C. C. Kan, M. L. Dalida, C. Pascua, M. W. Wan. Fixed-bed column studies on the removal of copper using chitosan immobilized on bentonite, Carbohydr. Polym. 83 (2011) 697-704.

[24] C. L. de Vasconcelos, B. M. Bezerril, D. E. S. dos Santos, T. N. C. Dantas, M. R. Pereira, J. L. C. Fonseca, Effect of molecular weight and ionic strength on the formation of polyelectrolyte complexes based on poly(methacrylic acid) and chitosan, Biomacromolecules, 7 (2006) 1245–1252.

[25] R. S. Vieira, M. M. Beppu, Interaction of natural and crosslinked chitosan membranes with Hg(II) ions, Colloids Surf. A., 279 (2006) 196–207.

[26] O. A. C., Jr. Monteiro, C. Airoldi, Some studies of crosslinking glutaraldehyde interaction in a homogeneous system, Int. J. Biol. Macromol., 26 (1999) 119–128.

[27] Z. J. Knaull, S. M. Hudson, A. M. K. Creber, Crosslinking of chitosan fibers with dialdehydes: proposal of a new reaction mechanism, J. Polym. Sci., 37 (1999) 1079–1094.

[28] N. Bilba, D. Bilba, G. Moroi, Synthesis of a polyacrylamidoxime chelating fiber and its efficiency in the retention of palladium ions, J. Appl. Polym. Sci., 92 (2004) 3730–3735.

[29] D. A. Fadel, L. A. Shouman, R. M. Afify, Selective transport of chromium (III), cobalt (II), barium (II) and strontium (II) ions through polymer inclusion membranes, Desalination Water Treat., 103 (2018) 163–174.

[30] F. Eloy, R. Lenaers, The chemistry of amidoximes and related compounds, Chem. Rev., 62 (1962) 155-183.

[31] I. Langmuir, The adsorption of gases on plane surfaces of glass, mica and platinum, J. Am. Chem. Soc., 40 (1918) 1361–1403.

[32] T. W. Weber, R. K. Chakravot, Pore and solid diffusion models for fixed bed adsorbents, AIChE J., 20 (1974) 228–238.

[33] A. Sari, M. Tuzen, D. Citak, M. Soylak, Equilibrium, kinetic and thermodynamic studies of adsorption of Pb(II) from aqueous solution onto Turkish kaolinite clay, J. Hazard. Mater., 149 (2007) 283–291.

[34] X. S. Wang, J. Huang, H. Q. Hua, J. Wang, Y. Qin, Determination of kinetic and equilibrium parameters of the batch adsorption of Ni(II) from aqueous solutions by Na-mordenite, J. Hazard. Mater, 142 (2007) 468–476.

[35] H. Freundlich, Adsorption in solution, Phys. Chem. Soc., 40 (1906) 1361–368.

[36] M. J. Temkin, V. Phyzev, Recent modifications to Langmuir isotherms, ActaPhysiochim. U. S. S. R., 12 (1940) 217–222.

[37] Y. S. Ho, Citation review of Lagergren kinetic rate equation on adsorption reactions, Scientometrics, 59 (2004) 171–177.

[38] Y. S. Ho, Review of second-order models for adsorption systems, J. Hazard. Mater., 136 (2006) 681–689.

[39] W. J. Weber, J. C. Morris, Equilibria and capacities for adsorption on carbon, J. Sanitary Eng. Div., 90 (1964) 79–108.

[40] C. Sarici-Ozdemir, Y. Onal, Equilibrium, kinetic and thermodynamic adsorptions of the environmental pollutant tannic acid onto activated carbon, Desalination, 251 (2010) 146–152.

[41] A. Nilchi, R. Saberi, M. Moradi, H. Azizpour, R. Zarghami, Adsorption of cesium on copper hexacyanoferrate–PAN composite ion exchanger from aqueous solution, Chem. Eng. J., 172 (2011) 572–580.

[42] S. M. El-Bahy, Z. M. El-Bahy, Synthesis and characterization of a new iminodiacetate chelating resin for removal of toxic heavy metal ions from aqueous solution by batch and fixed bed column methods, Korean J. Chem. Eng, 33 (2016) 2492–2501.

[43] S. M. El-Bahy, Z. M. El-Bahy, Synthesis and characterization of polyamidoxime chelating resin for adsorption of Cu(II), Mn(II) and Ni(II) by batch and column study, J. Environ. Chem. Eng. 4 (2016) 276–286.

[44] M. Christine, U. F. Sala, U. P. Sala, Quantitative determination of hexavalent chromium in aqueous solutions by UV-Vis spectrophotometer, Cent. Eur. J. Chem., 5 (2007) 1083-1093.

[45] N. Yahaya, I. Abustan, M. Latiff, O. Solomon Bello and M. A. Ahmad, Fixed-bed column study for Cu (II) removal from aqueous solutions using rice husk based activated carbon, Inter. J. Eng. Technol., 11 (2011) 248-252.

[46] A. Shahbazi, H. Younesi, A. Badiei, Batch and fixed-bed column adsorption of Cu(II) and CD(II) from aqueous solution onto functionalized SBA-15mesoporoussilica, Can. J. Chem. Eng., 91 (2013) 739–750.

[47] S. Singha, U. Sarkar, S. Mondal, Transient Behavior of a Packed Column of Eichhornia Crassipes stem for the Removal of Hexavalent Chromium, Desalination, 297 (2012) 48-58.

[48] Oualid Hamdaoui, Dynamic sorption of methylene blue by cedar sawdust and crushed brick in fixed bed columns, J. Hazard. Mater., 138 (2006) 293-303.

[49] R. Han, D. Ding, Y. Xu, W. Zou, Y. Wang, Y. Li, L. Zou, Use of rice husk for the adsorption of congo red from aqueous solution in column mode, Bioresour Technol., 99 (2008) 2938-46.

[50] R. Hana, Y. Wang, X. Zhaoc, Y. Wang, F. Xieb, J. Chengb, Mingsheng, Adsorption of methylene blue by phoenix tree leaf powder in a fixed-bed column: experiments and prediction of breakthrough curves, Desalination, 245 (2009) 284-297.

[51] M. Calero, F. Hernáinz, G. Blázquez, G. Tenorio, M. A. Martín-Lara, Study of Cr(III) biosorption in a fixed-bed column, J. Hazard. Mater, 171 (2009) 886-893.

[52] G. S. Bohart, E. Q. Adams, Some aspects of the behavior of charcoal with respect to chlorine, J. Chem. Soc. 42 (1920) 523–544.

[53] S. Chen, Q. Yue, B. Gao, Q. Li, X. Xu, K. Fu, Adsorption of hexavalent chromium from aqueous solution by modified corn stalk: A fixed-bed column study, Bioresour. Technol. 113 (2012) 114–120.

[54] H. Patel, R. T. Vashi, Fixed bed column adsorption of ACID Yellow 17 dye onto Tamarind Seed Powder, Can. J. Chem. Eng. 90 (2012) 180–185.

[55] Thomas, H. C., Heterogeneous ion exchange in a flowing system, J. Am. Chem. Soc., 66 (1944) 1664-1666.

[56] Yoon, Y. H., J. H. Nelson, Application of gas adsorption kinetics. I. A theoretical model for respirator cartridge service life, Am. Ind. Hyg. Assoc. J., 45 (1984) 509-516.